Senior Honors Thesis

The Heisenberg Model for 2D Spin-½ Triangular Antiferromagnets: An Application to Cs_2CuBr_4

Nicholas Squires
University of California, Davis

Abstract

The Heisenberg model was used to analyze the properties of the quasi two dimensional (2D) spin-½ triangular antiferromagnet Cs_2CuBr_4. High temperature series expansions of the magnetic susceptibility, Padé approximants, D-Log Padé approximants, and least squares analysis were used to determine diagonal nearest neighbor (J_1) and nearest neighbor (J_2) exchange constants, the Lande factors (g), the saturation field (H_s), and to provide evidence of spin frustration in this system. The theoretical calculations of these quantities are close to those determined by experiments, but are not close enough to conclude that Cs_2CuBr_4 is completely described by this model.

1. Introduction

High temperature and organic superconducting materials are one of the most exciting, and possibly one of the most important recent discoveries in all of science. The numerous possible applications of these novel materials such as superconducting transmission lines and high critical temperature (T_c) magnets, is just one of many reasons why they have captured the interest of materials scientists, chemists, and physicists alike. However, not enough is understood about the physical mechanisms that give these the extraordinary properties; thus limiting their practical applications.

On a macroscopic level, high temperature superconductors are often flaky ceramics that are poor metals (conductors) at room temperature. At the molecular level, many of them have planes of Copper or Oxygen atoms. At stoichiometry the 2D lattices in these planes act as antiferromagnetic insulators. Upon doping, and if its temperature is lowered sufficiently to its T_c, it enters a superconducting phase in which there is zero electrical resistance. Most of the superconducting "action" takes place within the planes; therefore, there is great interest in understanding the magnetic properties of the 2D antiferromagnetic structures that exist within these planes.

Over the past 15 -20 years, there has been significant theoretical and experimental work done on the properties of spin-½ triangular antiferromagnets (TAF's). These are magnetic structures that exist in the planes of some organic superconductors. They are antiferromagnets in which atoms having net spin of a half are situated on a triangular lattice. Experiments have been used to measure important magnetic properties in spin-½ TAF's such as exchange constants, g factors, and the saturation field. However, neutron scattering

experiments that can be used to accurately determine the exchange constants in a given superconducting material, are difficult and expensive to perform because they require extremely pure samples which are often very difficult to manufacture, especially in the case of organic crystals. On the other hand, bulk measurements such as the magnetic susceptibility (χ) and the specific heat as functions of temperature, are relatively easier to perform and can be determined quite accurately. The job of theoretical physicists is to come up with a quantitative prediction for these quantities to interpret the experiments and to determine the material's parameters.

In this paper, I first discuss some background information regarding, the nature of antiferromagnets, the exchange interaction, and the Heisenberg model. Next, I discuss past experimental and theoretical developments in the study of spin-½ TAF's including the phenomenon of frustration and its effect on magnetic ordering, high temperature series expansions of χ, and Padé and D-Log Padé approximants of χ. The remainder of the paper focuses on using these high temperature series approximations (obtained from the Heisenberg model for an anisotropic spin-½ TAF), experimental measurements of $\chi(T)$, and numerical and computational analysis to determine the exchange constants, g factors, and saturation field in Cs_2CuBr_4.

2. Antiferromagnetic Ordering and the Exchange Interaction

When the temperature of an antiferromagnetic crystal is lowered sufficiently it undergoes a phase transition from a disordered paramagnetic phase to an ordered antiferromagnetic phase. The temperature at which this occurs is called the Néel temperature (T_N), which is different for each material. Above its Néel temperature, molecular moments in the crystal are randomly aligned resulting in zero net magnetization. The magnetic susceptibility of the crystal above T_N is given by the Curie-Weiss law,

$$\chi(T) = \frac{C}{T + T_N'} \tag{1}$$

where C, (the Curie constant) and T_N' are material dependent constants. Note that there is no divergence in the susceptibility as it reaches the transition temperature since $T_N' > 0$. In the case of a ferromagnetic crystal, there is a divergence in the susceptibility as it transitions from a paramagnetic to ferromagnetic phase. At T_N the molecular moments become spontaneously aligned anti-parallel to their neighboring spins also resulting in a net magnetization of zero. Since there is no net magnetization in either phase, how are they distinguished from one another?

Consider the ionic crystal MnF_2 which has chemical notation $Mn^{2+}F_2^-$. It crystallizes in the face-center cubic structure as shown in figure 1.

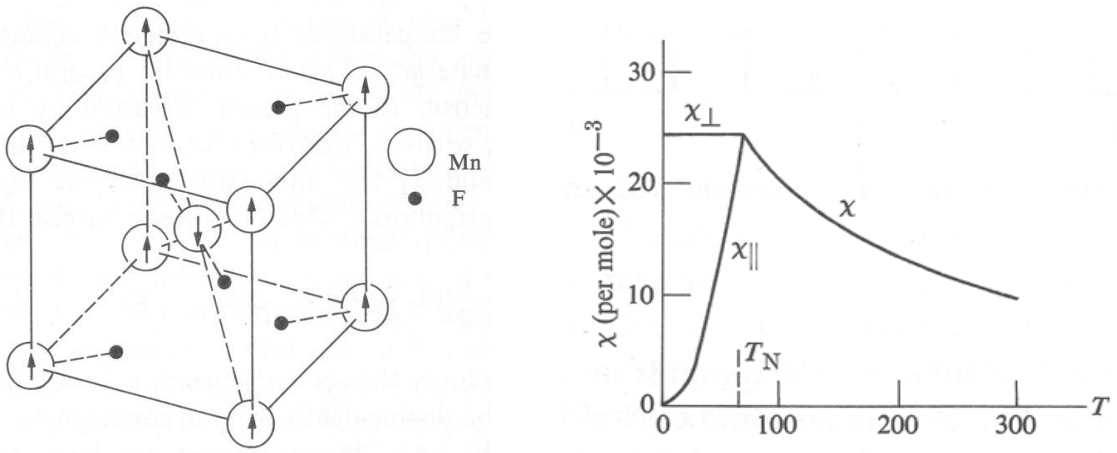

FIG. 1 (Omar, p. 451) (Left). (fcc) Crystal structure of MnF_2. The arrows on the Mn^{2+} ions indicate the direction of the magnetic moment, illustrating their antifferomagnetic arrangement. FIG. 2 (Omar, p. 452) on the right illustrates the susceptibility curve for MnF_2 . Its paramagnetic phase exists up to T_N, below which the susceptibility behaves as shown with the field applied perpendicular ($\perp$) and parallel ($\|$) to the direction of the moments.

The manganese and fluorine ions have ground state electron configurations $[Ar]3d^3 4s^2$ and $[He]2s^2 2p^6$ respectively; the square brackets denote core electron configurations. The fluorine ions are not magnetic since they have a filled outer 2p shell, while the manganese ions are magnetic due to their unfilled 3d shell. This crystal is antiferromagnetic since the manganese ions at the corners of the unit cell have moments aligned anti-parallel to the manganese ions at the center of the unit cell.

A paramagnet obeys the Curie law $\chi \sim 1/T$ for all temperatures, while the susceptibility of an antiferromagnet below T_N behaves as illustrated in figure 2. $\chi_\perp$ corresponds to a magnetic field applied perpendicular to the spin alignment and $\chi_\|$ corresponds to a magnetic field applied parallel to the orientation of the moments. The paramagnetic phase of MnF_2 can thus be distinguished from its antiferromagnetic phase, by examining the susceptibility plot in figure 2. Thus, the characteristic behavior of the susceptibility as a function of temperature provides a mechanism for distinguishing between unordered and ordered phases in antiferromagnets.

Spontaneous anti-alignment of molecular moments in antiferromagnets implies the presence of an internal field. This internal field is called the molecular field. In 1928, Heisenberg proposed that the molecular field responsible for the magnetic ordering in solids is the result of a spin dependent exchange interaction between moments on neighboring lattice sites. Furthermore, he proposed that the exchange (potential) energy between atoms of net spin $\mathbf{S_i}$ and $\mathbf{S_j}$ on neighboring sites is given by,

$$V_{ij} = J_{ij}\, \mathbf{S_i} \cdot \mathbf{S_j} \tag{2}$$

where J_{ij} is the corresponding exchange constant and (for spin ½ atoms),

$$\mathbf{S_i} = \frac{\hbar}{2}\boldsymbol{\sigma_i} \tag{3}$$

with $\boldsymbol{\sigma_i}$ being the Pauli spin matrices. Consequently, if $J_{ij} > 0$ the lowest energy configuration is when the spins are aligned anti-parallel to one another, corresponding to

antiferromagnetic ordering of the moments. In the case where $J_{ij} < 0$, the lowest energy configuration occurs when spins are aligned parallel to one another, resulting in a ferromagnetic ordering of the moments.

The physical origin of the exchange energy is governed by the laws of quantum mechanics. Electrons interact classically via Coulomb's law, and quantum mechanically via the Pauli Exclusion Principle. The Pauli Exclusion Principle prohibits electrons with like spins from coming close to one another which in effect reduces their coulomb repulsion. On the other hand, electrons with opposite spins can get close to one another resulting in a higher coulomb repulsion between them. The exchange energy can then be thought of as the difference in potential energy of the parallel and anti-parallel spin states. This spin dependent exchange energy is responsible for magnetic ordering in materials.

3. The Heisenberg Model

The Heisenberg model consists of a Hamiltonian for an array of spins with the exchange energy given in (2). That is, the exchange interaction between all moments on the lattice contributes a term of the form (2) to the Hamiltonian. The result is a many-body Hamiltonian due to the large number of exchange interactions that must be considered (i.e. there is on the order of 10^{23} moments). The Heisenberg Hamiltonian for the system is,

$$\mathcal{H} = \sum_{j} J_{ij}(\mathbf{S_i} \cdot \mathbf{S_j}) \tag{4}$$

where $\mathbf{S_i}$ and $\mathbf{S_j}$ are spin-½ operators, and the sum over j indicates summation over all atoms relative to the reference spin i.

Exchange interactions fall off rapidly with increasing distance; thus it is sufficient to only consider nearest neighbor exchange interactions. The term nearest neighbors means the moments which are physically closest to one another on a crystal lattice. On the hypothetical square lattice in figure 3 the pairs of moments at lattice sites 1 and 2 and at sites 1 and 3 are nearest neighbors pairs.

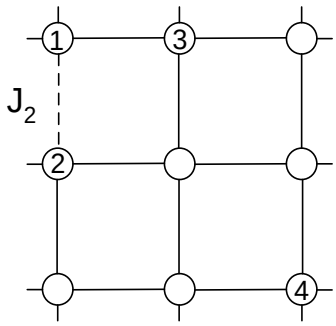

FIG 3. Spin-½ atoms situated on a square lattice. Atoms 1 and 3, and 1 and 2 are nearest neighbors

The reason why the exchange interactions fall of rapidly with distance has to do with their underlying physical nature. Exchange interactions between electrons are spin-

dependent forces arising from both Coulomb interactions and the Pauli Exclusion Principle, which they are subject too. The Coulomb interaction acts at a long range so that even electrons far apart are influenced by one another's electric field. The magnitude of the Coulomb repulsion is on the order of r^{-2}, where r is the distance between the electrons. However, for the Pauli Exclusion Principle to be a significant effect on a pair of electrons, they must be able to come very close to one another. Electron's whose wave functions have significant overlap, have the best chance of coming close to one another and thus the best chance of interacting via the Exclusion Principle.

An electron's wave function decays rapidly away from the electron. With few exceptions outer shell electrons in atoms 1 and 4, (see figure 3), will have a smaller amount of overlap of their wave functions compared with amount of overlap of electronic wave functions in nearest neighbor atoms 1 and 2. This leads to the conclusion that exchange interaction beyond those of the nearest neighbor type are relatively small, and can thus be neglected.

4. The Heisenberg Model for 2D Spin-½ TAF's and Frustration

A 2D spin-½ TAF is an antiferromagnetic crystal in which atoms, having net spin of a half are situated on a triangular lattice. A hypothetical triangular lattice is shown in figure 4.

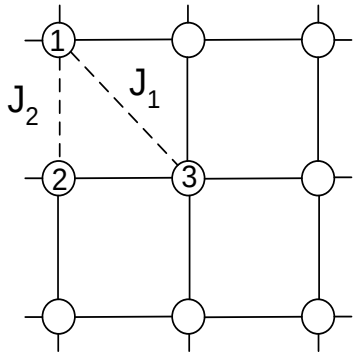

FIG. 4. Hypothetical triangular lattice. J_2 and J_1 are nearest neighbor and diagonal nearest neighbor exchange constants respectively.

The model relevant to our study here includes exchange interactions of both nearest neighbor (NN) and diagonal nearest neighbor (DNN) moments. The dashed lines in figure 4 between the moments at lattice sites 1 and 2 and between 1 and 3 indicate nearest neighbor and diagonal nearest neighbor interactions respectively. J_2 and J_1 are the exchange constants for these NN and DNN interactions respectively. The Hamiltonian for this system is,

$$\mathcal{H} = J_1 \sum_{<ij>} \mathbf{S_i} \cdot \mathbf{S_j} + J_2 \sum_{<ik>} \mathbf{S_i} \cdot \mathbf{S_k} \tag{5}$$

where the summation over <ij> and <ik> indicate sums over DNN's and NN's respectively. Figure 5 illustrates an isotropic triangular lattice which results if $J_1 = J_2 \neq 0$. In this case, the

Hamiltonian (5) is reduced to a single sum. In the case where $J_1 \neq J_2 \neq 0$, the triangular lattice is distorted or anisotropic, and the Hamiltonian is given by (5).

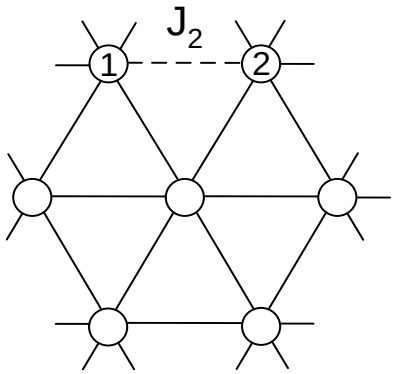

FIG. 5. Isotropic triangular lattice

In an antiferromagnet, neighboring moments want to align anti-parallel to one another. The geometry of a square lattice, allows the moments to attain perfect antiferromagnetic ordering as shown in figure 6(a). On the other hand, the geometry of a triangular lattice does not allow for perfect antiferromagnetic ordering of the moments. Figure 6(b) illustrates that it is possible for the moments at lattice site 1 and 2 to align anti parallel, but the moment at lattice site 3 can not be placed exactly anti parallel to the other two; there cannot be perfect antiferromagnetic alignment on a triangular lattice. Thus, a TAF is said to be frustrated, an effect which leads to many interesting ordered phases in a TAF.

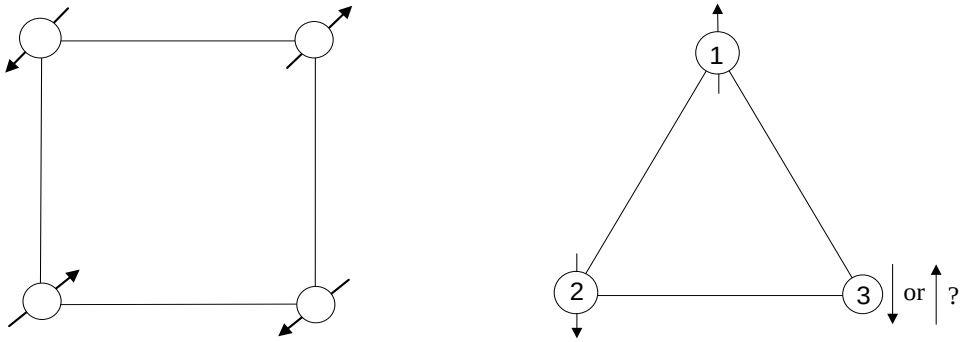

FIG. 6. (a) (left) The geometry of a square lattice allows for perfect antiferromagnetic (AF) alignment of the spins so that nearest neighbors are aligned anti parallel to one another. The geometry of the triangular lattice (b) (right) prohibits perfect AF ordering since spin 3 cannot be aligned anti parallel to both of its nearest neighbors 1 and 2. The system is said to be frustrated.

5. Heisenberg Hamiltonian for an Anisotropic Spin-½ TAF in an Applied Magnetic Field

Associated with the magnetic field on a molecular moment is the orientational potential energy,

$$V = - \boldsymbol{\mu} \cdot \mathbf{H} = -g \mu_B H S^z \tag{6}$$

H is the magnitude of the magnetic field (taken to be applied in the z direction), μ_B is the Bohr Magneton, $S^z = +/- ½$, and g is the Lande factor given by,

$$g = 1 + \frac{j(j+1) + s(s+1) - l(l+1)}{2j(j+1)} \tag{7}$$

where *l*, *s*, and *j*, are the orbital, spin, and total angular momentum quantum numbers respectively. The Lande factor describes the origin of angular momentum in the system. For example, in the case of pure orbital motion $s = 0$ so that $j = l$, resulting in $g = 1$. In the case of pure spin motion $l = 0$ so that $s = j$, and $g = 2$.

In the presence of a magnetic field, applied in the z direction, the moments on a triangular lattice tend to align in the in the z direction. The orientation potential energy of each moment must be factored into the Hamiltonian so that (5) becomes,

$$\mathcal{H} = J_1 \sum_{<ij>} \mathbf{S_i} \cdot \mathbf{S_j} + J_2 \sum_{<ik>} \mathbf{S_i} \cdot \mathbf{S_k} - Hg\mu_B \sum_i \mathbf{S_i}^z \tag{8}$$

where the sum over i, is over all molecular moments. From this equation, we see that when $J_1 > 0$ and $J_2 > 0$ (both interactions are antiferromagnetic), there is competition between the antiferromagnetic exchange interaction which fights to keep neighboring moments in an anti parallel arrangement, and the spin field coupling which fights to align the moments parallel to the field and incidentally parallel to one another.

6. Field Induced Ordered Phases in a 2D Isotropic Spin-½ TAF

The Hamiltonian for an isotropic spin-½ TAF in an applied magnetic field (in z direction) is given by,

$$\mathcal{H} = \sum_{<ij>} J_{ij} \mathbf{S_i} \cdot \mathbf{S_j} - Hg\mu_B \sum_i \mathbf{S_i}^z \tag{9}$$

This Hamiltonian can be used to shed light on how the spins are ordered for different magnitude ranges of an applied field. Consider three spins on a triangular lattice as shown below in figure 7.

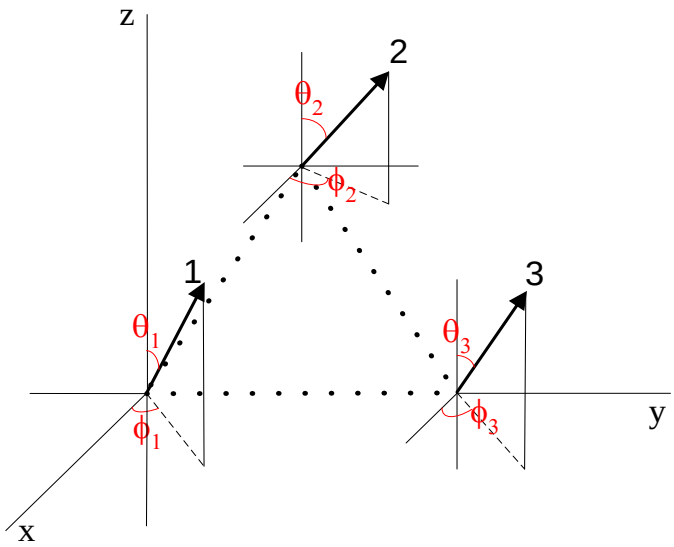

FIG. 7. Arrangement of spins on a triangular lattice. The spins are taken to be unit vectors with their orientations in space given by the angles θ and ϕ (spherical coordinates). θ varies between 0 and π, while ϕ vaires between 0 and 2π

For simplicity, assume the spins are unit vectors. Spin 1 makes an angle of θ_1 and ϕ_1 to the z and x axis's respectively, while spins 2 and 3 make similar angles to these axis. The components of spin 1 in rectangular coordinates are ($\sin\theta_1\cos\phi_1$, $\sin\theta_1\sin\phi_1$, $\cos\theta_1$); the positions of spins 2 and 3 are given by similar expressions. Taking the exchange constants to be unity (still antiferromagnetic exchange interactions), we can take the total energy of the system to be,

$$E_{total} = \mathbf{S_1}\cdot\mathbf{S_2} + \mathbf{S_2}\cdot\mathbf{S_3} + \mathbf{S_1}\cdot\mathbf{S_3} - Hg\mu_B(\mathbf{S_1}^z + \mathbf{S_2}^z + \mathbf{S_3}^z) \qquad (10)$$

where S^z's are the z component of each spin vector. Note that the z-component can be written as $S_x{}^z = \cos\theta_x$. The scalar products in (10) can be computed directly resulting in an expression in terms of the angles θ and ϕ. For example,

$$\mathbf{S_1}\cdot\mathbf{S_2} = \sin\theta_1\sin\theta_2\cos(\phi_1 - \phi_2) + \cos\theta_1\cos\theta_2 \qquad (11)$$

with the scalar products $\mathbf{S_1}\cdot\mathbf{S_3}$ and $\mathbf{S_2}\cdot\mathbf{S_3}$ yielding similar expressions. After making these substitutions into the total energy of the system, it becomes clear that the energy of the system is dependent solely on the angles θ, ϕ, and on the magnitude of the magnetic field H (since g (=2) and μ_B are constants). From this point, a computer program can be used to determine the lowest energy configurations of the spins for various values of H. A possible algorithm is given in Appendix A. This program will output the lowest energy configurations (ordered phases) of the spins by determining the angles θ and ϕ for each spin, which minimize the total energy, for each value of H.

The possible ordered phases are those shown in figures 8(a) – 8(d).

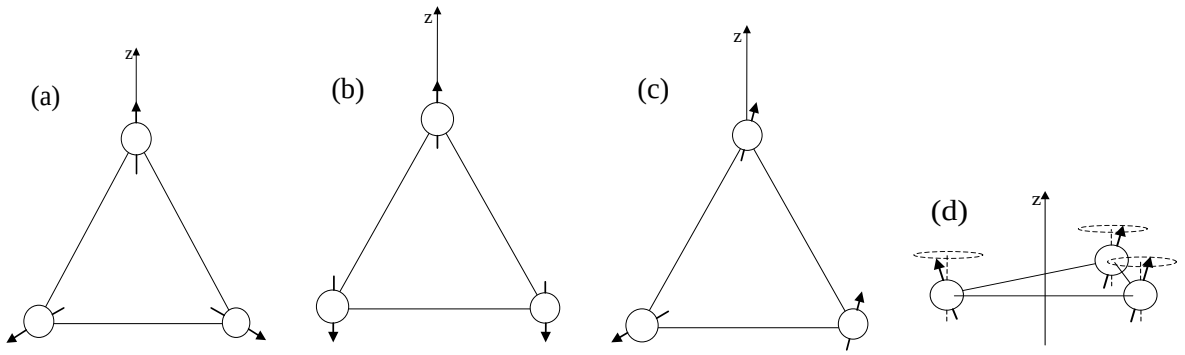

FIG. 8(a)-(d). Possible ordered phases in a TAF, derived from simplified expression for the total energy of the system (12).

Figures 8(a) and 8(c) are coplanar structures (spins lie in the same plane), 8(b) is a collinear structure (all spins lie along same line), and 8(d) is an umbrella structure, where the spin is allowed to rotate freely about the direction of the applied field [1,2].

An important quantity when studying magnetic systems is the magnetization (M). It is defined as the magnetic moment per unit volume. The magnetization is also known as an order parameter, since it is a measure of how well the moments are aligned. A schematic magnetization curve for this spin system is shown in figure 9.

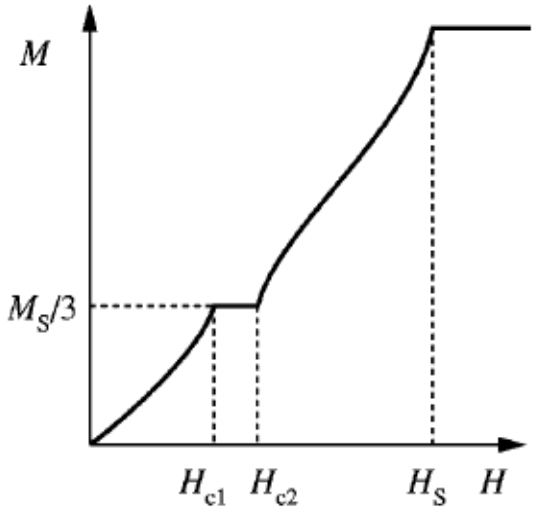

FIG. 9. [1] Schematic magnetization curve for a spin-½ TAF. The various spin structures are stabilized for different ranges of the magnetic field. There is a magnetization plateau at one third the saturation magnetization M_s.

The spin structure in figure 8(a) occurs for $H < H_{c1}$, the structure in 8(b) occurs for $H_{c1} < H < H_{c2}$, the structure in 8(c) for $H_{c2} < H < H_s$, and the umbrella structure is not an optimal configuration [1]. At H_s, the torque on the moments is so great that that they are forced into a ferromagnetic ordering. This behavior of the magnetization in a varying magnetic field was observed experimentally for Cs_2CuBr_4 [1], providing evidence that it contains spin-½ TAF's in its planes.

7. High Temperature Series Expansions of χ

The magnetic susceptibility is defined as,

$$\chi = \frac{\partial M}{\partial H} \tag{12}$$

It is a measure of how fast the magnetization changes with a varying magnetic field. This quantity is important in our study because it is related to the exchange constants of a system described by (5). To see how they are related, we begin with the expression for the zero field molar susceptibility for N atoms on a lattice (Ashcroft, p.710),

$$\chi_{molar} = N_A g\mu_B \frac{\partial}{\partial H} < \sum_i \mathbf{S_i}^z > \Big|_{H=0} \tag{13}$$

where N_A is Avogadro's number. The notation χ will be used from here on to denote the molar susceptibility, unless otherwise stated. Taking the $\mathbf{S_i}$'s to be spin-½ operators; the ground state expectation value (denoted by the angular brackets) is defined by,

$$< \mathbf{S_i}^z >= \frac{Tr(\mathbf{S_i}^z e^{-\beta\mathcal{H}})}{Tr(e^{-\beta\mathcal{H}})} \tag{14}$$

where "Tr" represents the trace (sum of the diagonal elements) of a matrix, and $\mathcal{H}$ is the Hamiltonian (8). Carrying out the differentiation in (13) with respect to H yields,

$$\chi = \frac{N_A (g\mu_B)^2}{k_B T} < \sum_j \mathbf{S_i}^z \mathbf{S_j}^z > \Big|_{H=0} \tag{15}$$

where k_B is the Boltzman constant.

A closed form solution of (15) with the Hamiltonian defined by (8) has yet to be found. The difficulty in finding a closed form solution is evident from the expression (14); it requires exponentiation of a Hamiltonian which is not diagonal. However, an approximate solution can be found for high temperatures, using a Taylor expansion of the exponential term. Letting i = 0 so that $\mathbf{S_0}^z$ is the reference spin (this can be any spin on the lattice), for high temperatures (15) is,

$$\chi = \frac{N_A (g\mu_B)^2}{k_B T} \sum_j \frac{Tr[\mathbf{S_0}^z \mathbf{S_j}^z (1 - \beta\mathcal{H} + \frac{(\beta\mathcal{H})^2}{2!} - \frac{(\beta\mathcal{H})^3}{3!} + \ldots)]}{Tr[(1 - \beta\mathcal{H} + \frac{(\beta\mathcal{H})^2}{2!} - \frac{(\beta\mathcal{H})^3}{3!} + \ldots)]} \tag{16}$$

where $\beta = 1/k_B T$.

The next task is to calculate the coefficients in this expansion, which turns out to be a difficult task for orders of β greater than one. Keeping only the first term in this expansion, (i.e. β^0) (16) becomes,

$$\chi = \frac{N_A (g\mu_B)^2}{k_B T} \sum_j \frac{Tr[\mathbf{S_0}^z \mathbf{S_j}^z (1)]}{Tr(1)} \tag{17}$$

Since $\mathbf{S_0}^z$ and $\mathbf{S_j}^z$ are spin-½ operators we have,

$$Tr[\mathbf{S_0}^z \mathbf{S_j}^z (1)] = ¼ \delta_{0j} Tr(1) \tag{18}$$

where δ is the standard Kronecker delta notation. Thus, the sum in (17) is equal to ¼Tr(1) x $[Tr(1)]^{-1}$; since every term in the sum is zero except when j = 0. Finally, the terms Tr(1) in the numerator and denominator cancel out (note: $Tr(1) = 2^N$ where N is the number of lattice sites) and the susceptibility becomes,

$$\chi = \frac{N_A (g\mu_B)^2}{k_B T} \frac{S(S+1)}{3} \tag{19}$$

which is a Curie law (χ~1/T) describing the susceptibility of the antiferromagnet in its disordered paramagnetic phase at high temperatures[{1}]. If this Curie susceptibility were valid for all temperatures (T), then the susceptibility would diverge as T approaches zero. This has been shown experimentally to be false (figure 2 shows this for MnF_2). This assumption cannot be made from a mathematical stand point since the Taylor expansion itself is only valid for high T (small β).

To obtain a more accurate expression for the susceptibility of this system, higher ordered terms in the expansion need to be included. If both the β^0 and β^1 terms are included in the expansion, then,

$$\chi = \frac{N_A (g\mu_B)^2}{k_B T} \sum_j \frac{Tr[\mathbf{S_0}^z \mathbf{S_j}^z (1 - \beta\mathcal{H})]}{Tr(1 - \beta\mathcal{H})} \tag{20}$$

where $\mathcal{H}$ is the Hamiltonian (5). Rearranging (20) we have,

$$\chi = \frac{N_A (g\mu_B)^2}{k_B T} \sum_j \frac{Tr(\mathbf{S_0}^z \mathbf{S_j}^z) - \beta Tr[(\mathbf{S_0}^z \mathbf{S_j}^z)\mathcal{H}]}{Tr(1) - \beta Tr(\mathcal{H})} \tag{21}$$

The first term in the numerator is given by (18). Furthermore, the denominator is just Tr(1) since $Tr(\mathcal{H}) = 0$. Thus we only need to calculate the second term in the numerator. Plugging (5) in we have,

[{1}] The ¼ in (18) is written as S(S+1)/3 where S is the spin quantum number. Here S = ½.

$$\mathrm{Tr}[(\mathbf{S_0}^z\mathbf{S_j}^z)\mathcal{H}] = J_1(\sum_n \mathrm{Tr}(\mathbf{S_0}^z\mathbf{S_j}^z\mathbf{S_0}\cdot\mathbf{S_n})) + J_2(\sum_m \mathrm{Tr}(\mathbf{S_0}^z\mathbf{S_j}^z\mathbf{S_0}\cdot\mathbf{S_m})) \tag{22}$$

with $\mathbf{S_0}\cdot\mathbf{S_n}$ = $(S_0^xS_n^x + S_0^yS_n^y + S_0^zS_n^z)$. Since different components of the spin are uncorrelated, (23) reduces to,

$$\mathrm{Tr}[(\mathbf{S_0}^z\mathbf{S_j}^z)\mathcal{H}] = \frac{1}{4}\left[1-\frac{\beta}{4}(q_1J_1+q_2J_2)\right] \tag{23}$$

where q_1 and q_2 are the number of DNN's and NN's respectively. Spin 0 has a total of six neighboring spins, where $q_1 = 2$ and $q_2 = 4$.

Plugging (23) into (21) and performing some simplifications, we get the first order correction to the magnetic susceptibility,

$$\chi = \frac{\frac{N_A(g\mu_B)^2}{k_B}\frac{S(S+1)}{3}}{T+\left[\frac{S(S+1)}{3k_BT}(q_1J_1+q_2J_2)\right]} \tag{24}$$

This is the Curie-Weiss law given in (1) where C is the quantity in the numerator, and T_N' is the quantity in square brackets in the denominator.

When even higher terms are kept in the expansion, it becomes increasingly difficult to determine the coefficients. This difficulty arises for orders of β greater than 1 since the Hamiltonian is no longer linear, and terms having the form $\mathrm{Tr}(S_0^zS_j^z\,\mathcal{H}^2)$ must be computed.

The goal is to determine the relationship between the susceptibility and the exchange constants J_1 and J_2. The approximation (19) does not reveal this relationship; however keeping more terms in the series expansion does. The first order correction to χ, equation (24), shows that the susceptibility is a function of the exchange constants.

In effect, we have created a power series representation for $\chi * k_BT$ in powers of β,

$$\chi(\beta) * k_BT = \sum_n \frac{1}{n!}a_n(J_1,J_2)\beta^n \tag{25}$$

For n = 0 and n = 1 we found,

$$a_0 = N_A(g\mu_B)^2\frac{S(S+1)}{3} \tag{26}$$

$$a_1 = N_A(g\mu_B)^2(q_1J_1+q_2J_2)\left[\frac{S(S+1)}{3}\right]^2 \tag{27}$$

Determining higher coefficients in (25) requires sophisticated computational methods. In my analysis, I used a computer program from Dr. Zheng Weihong[{2}] ("program 1") that generates the coefficients in the expansion up to order β^9, for any ratio of the exchange constants, J_1/J_2.

When J_1 and J_2 are both greater than zero (antiferromagnetic interactions) the effect of the first order correction is to begin to flatten out the susceptibility curve. In modeling a real spin-½ TAF, the temperature at which the flattening takes place is the Néel temperature. At T_N, the decrease in entropy is sufficient enough that the exchange interactions become the dominant factor in determining spin alignment. That is, the spins begin to align anti parallel to one another indicating the systems transition from a paramagnetic phase to an ordered phase. We will see later that keeping even higher terms in the expansion causes the susceptibility curve to "turn down" (concave down) at low temperatures.

8. A More Accurate Expression for χ at Low Temperatures: Padé and D-Log Padé Approximations

As we know, the power series expansion for χ breaks down at low temperatures. We can use Padé and D-Log Padé approximants to improve the approximation at lower temperatures. In general, these approximation methods produce results that are superior to polynomial approximations (Burden, p. 517-518). In a Padé approximation, a polynomial of order s is approximated by a ratio of polynomials P and Q of order N and M respectively, such that N + M = s. Employing this method for the susceptibility,

$$\chi = \frac{P(\beta)}{Q(\beta)} = a_0 + a_1\beta + ... + a_s\beta^s = \frac{p_0 + p_1\beta + ... + p_N\beta^N}{q_0 + q_1\beta + ... + q_M\beta^M} \tag{28}$$

Note that for χ to be defined as $\beta \to 0$ (i.e high temperature limit), it must be true that $q_0 \neq 0$. Without loss of generality, q_0 is set to one. To determine the coefficients of P and Q we begin by multiplying both sides of (28) by the denominator on the right hand side,

$$(a_0 + a_1\beta + ... + a_s\beta^s)(q_0 + q_1\beta + ... + q_M\beta^M) = p_0 + p_1\beta + ... + p_N\beta^N \tag{29}$$

For this equation to be satisfied, the coefficients for like powers of β must be equal. Thus for $n \leq N$ we have the following N + 1 algebraic equations for the powers of β up to n,

$$\begin{aligned} &\beta^0 : a_0 = p_0 \\ &\beta^1 : a_0 q_1 + a_1 = p_1 \\ &... \\ &\beta^n : \sum_{i=0}^{n} a_i q_{n-i} = p_n \end{aligned} \tag{30}$$

[{2}] I would like to thank Dr. Weihong for providing us with this program.

Furthermore, since P is a polynomial of order N, all of its coefficients are zero for n > N. Thus we have the additional algebraic equations for n > N,

$$\beta^n : \sum_{i=0}^{n} a_i q_{n-i} = 0 \tag{31}$$

Note that the q_n's are zero for n > M, so that (31) leads to a system of algebraic equations. As an example, assume that we are given the expansion for χ up to order β^s, and that P is a polynomial of order β^N and Q is a polynomial of order β^M. In this case (31) leads to the system of equations below (written in matrix form),

$$\begin{pmatrix} a_0 & a_1 & a_2 & \dots & a_{M-1} \\ a_1 & a_2 & a_3 & \dots & \dots \\ a_2 & a_3 & a_4 & a_5 & \dots \\ \dots & \dots & a_5 & \dots & \dots \\ a_{M-1} & \dots & \dots & \dots & a_{s-1} \end{pmatrix} \begin{pmatrix} q_M \\ \dots \\ \dots \\ \dots \\ q_1 \end{pmatrix} = \begin{pmatrix} a_M \\ \dots \\ \dots \\ \dots \\ a_s \end{pmatrix} \tag{32}$$

where the a_s's are the coefficients from the expansion for χ. In shorthand notation, (32) can be written as $A\mathbf{q} = \mathbf{a}$. The coefficients of Q, are thus determined by the equation $\mathbf{q} = A^{-1}\mathbf{a}$; that is, inversion of the matrix A and subsequent multiplication by **a** yields the coefficients for Q. Once we have the q's, we can plug them into (30) along with the a_s's, and directly calculate each coefficient of P. Finally, the coefficients of P and Q are plugged into (28) resulting in an |N,M| Padé approximant of $\chi(\beta)$.

I was given a second program ("program 2") from Dr. Singh which computes the |N,M| Padé approximant for a given polynomial of any order, and evaluates this rational function at discrete steps in the in the functions variable. Here it was used to calculate the various Padé approximants for $T^*\chi(\beta)$ at discrete values of β[3]. To get χ as a function of T, the data must be inverted. First, the T values are found by taking the reciprocal of β at each step. Once these reciprocals are calculated, $\chi(T)$ is found by dividing $T^*\chi(\beta)$ by the reciprocals at each step. Doing this for every value in the set, results in a data set with $\chi(T)$ at discrete T values.

The possible Padé approximants for χ, a 9th order polynomial, are |1,8|, |8,1|, |2,7|, |7,2|, |3,6|, |6,3|, |4,5|, |5,4|. Figure 11 illustrates some of these approximants for $J_1/J_2 = 0.5$[4].

[3] In this program k_B is set to unity so that $\beta = 1/T$.
[4] The choice of J_1/J_2 here is arbitrary.

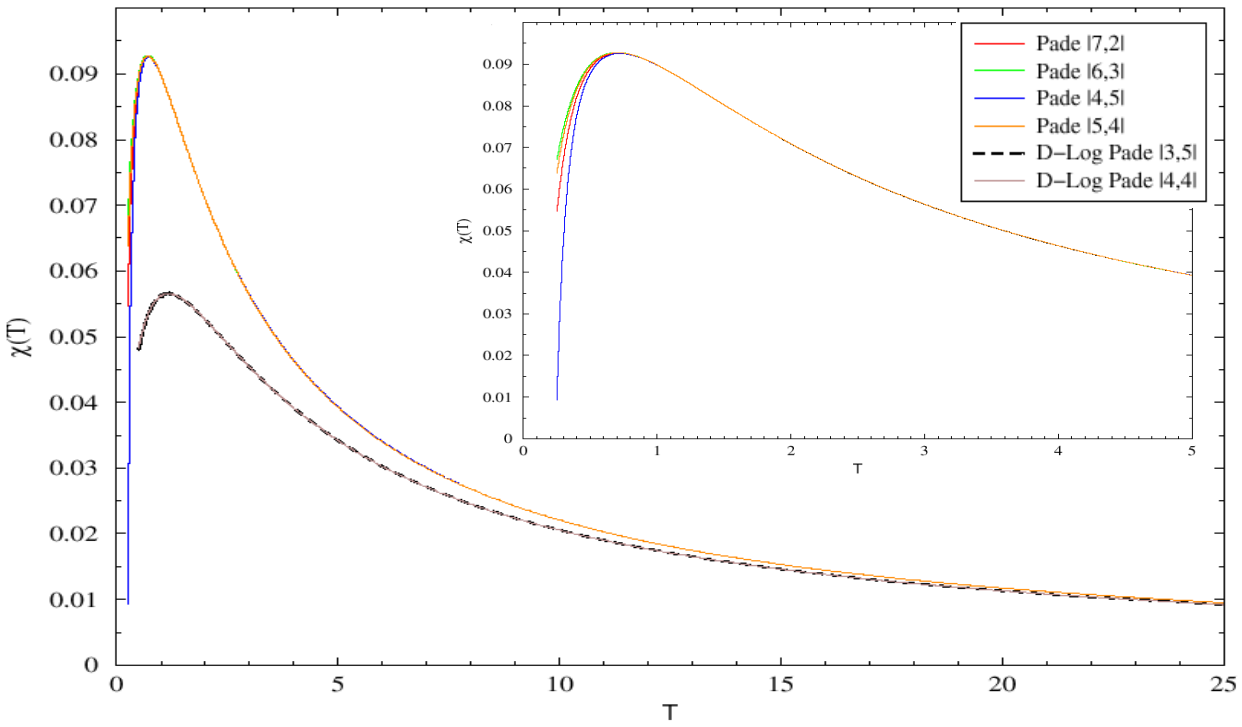

FIG. 11. Behavior of χ as a function of T for some of the Padé and D-Log Padé approximants that exhibit the characteristic behavior of χ(T) for a spin-½ TAF (See figure 13). The insert is a closer look at the Padé approximants illustrating their diverse behavior. The Padé and D-Log Padé approximants only begin to agree well at ~ 25 - 30.

There is a problem with Padé approximants. In general, the behavior of a function relies heavily on the nature of its singularities in the complex plane. The theory of critical phenomena predicts that the susceptibility has the general form (G. A. Baker, p.10)

$$\chi = \left(1 - \frac{T_c}{T}\right)^{\gamma} \tag{33}$$

In the Padé approximant for χ, its singularities come from the zeros of Q(β); thus they can only reliably up to a certain point. They are reliable up to the point where they agree well with D-Log Padé approximants of χ. The complicated singularities in the susceptibility function are removed by taking the derivative with respect to T of the natural logarithm of χ. That is

$$D(T) = \frac{d}{dT} \ln \chi(T) = \frac{-\gamma}{T - T_c} \tag{34}$$

The function D(T) has a simple pole at T_c and a residue of $-\gamma$; thus, it is better to use a Padé approximant for D(T) because it can handle more general types of singularities than the Padé approximants can.

The next problem is how to extract data from this expression in the same form as the data output of program 2; that is how to retrieve data sets with $T^*\chi(\beta)$ at discrete β values. Dr. Singh gave me another program ("program 3") which takes as input the coefficients from program 1 then performs the necessary numerical differentiations, Padé approximants, numerical quadrature, and outputs similar data sets as in program 2. The possible D-Log Padé approximants for D(T), which due to the differentiation is now only an 8^{th} order polynomial, are |1,7|, |7,1|, |2,6|, |6,2|, |3,5|, |5,3|, and |4,4|. Of these 8 approximants, only the |3,5| and |4,4| ones behave the same as the experimental susceptibility (see figure 13); these are plotted along with the Padé approximants in figure 11 for $J_1/J_2 = 0.5$.

The Padé approximants are only reliable up to the point where they agree well with the D-Log Padé approximants. In figure 11, we see that they begin to agree well at ~25-30. To produce a sufficient approximation, we need approximants that are reliable down to ~9 (see figure 13). The differences in susceptibility curves of the two types of approximations leads us to the conclusion that Padé approximants are insufficient in providing a suitable approximation; instead we must use D-Log Padé approximants to obtain a reliable approximation of the susceptibility at these temperatures.

D-Log Padé and Padé approximants for χ in the antiferromagnetic square lattice and 1-dimmensional chain limits, $J_1 = 0$ and $J_2 = 0$[{5}] respectively, provide further evidence that D-Log approximants are more reliable to use in our study. The susceptibility in both cases are accurately reported in [6,7]. In both limits, the susceptibility curve from the D-Log Padé approximants reproduced the results of these earlier studies very well; while the Padé approximants for χ did not agree well at all. Now that we know the D-Log Padé approximants are more reliable to use in general, to what extent is the D-Log Padé approximant itself reliable? For both $J_1 = 0$ and $J_2 = 0$, the approximation of χ begins to digress from the reported χ values at ~0.3 temperature units below their respective peak values; thus, we take them to be reliable down to $T = 0.3$.

9. Outline of Method Used to Determine the Exchange Constants and Lande Factors in Cs_2CuBr_4

Our goal is to approximate the exchange constants in a real 2D spin-½ TAF using the Heisenberg model and high temperature series expansions of χ. We examine the real spin-½ TAF Cs_2CuBr_4. We chose this material since we have access to experimental susceptibility data and since we can compare our theoretical results to those reported in recent studies for the values of its exchange constants [1].

The crystal structure of Cs_2CuBr_4 is shown in figures 12(a) and 12(b) along two different axes.

[{5}] The coefficients in susceptibility expansion could not be obtained directly from program 1. Instead, I obtained them from Dr. Singh.

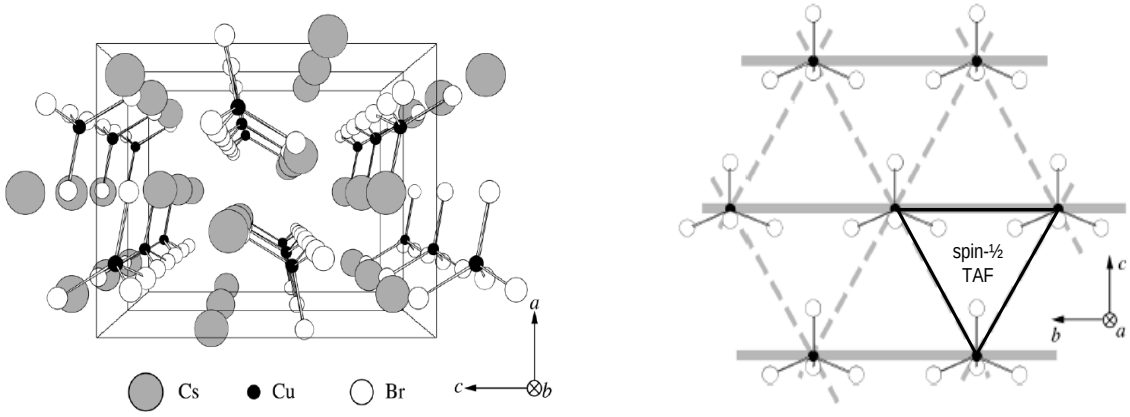

FIG. 12. [1]. (a) (left) Arrangement of ions in Cs_2CuBr_4. The solid gray lines indicate the unit cell. (b)(right) Arrangement of spin-½ Br^- ions (filled circles) in the bc plane. Their arrangement on the lattice forms a spin-½ TAF.

Its chemical notation is $Cs^+Cu^{2+}Br^-$. The Cs^+, Cu^{2+}, and Br^- ions have electron configurations $[Kr]4d^{10}5s^25p^6$, $[Ar]3d^9$, and $[Ar]\ 3d^{10}4s^24p^6$ respectively. The Br^- and Cs^+ ions have complete outer shells and therefore have no net spin. On the other hand, the Cu^{2+} ions have an incomplete 3d shell with one unpaired electron, resulting in a net spin of a half. Figure 12(b) illustrates the arrangement of Cu^{2+} ions in the bc planes; the bold lines indicate the formation of a an anisotropic spin-½ TAF. Recent neutron inelastic scattering experiments determined that nearest neighbor and diagonal nearest neighbor exchange interactions are dominant in a similar compound, Cs_2CuCl_4. In Cs_2CuCl_4, interlayer exchange interactions are less than $10^{-2} \times J_1$ [1]. Thus Cs_2CuCl_4 can be described as a quasi two dimensional TAF. Since Cs_2CuBr_4 has the same crystal structure as Cs_2CuCl_4, it is also assumed to be a quasi 2D TAF [1].

The method used here to determine the exchange constants, Lande factors, and saturation field of Cs_2CuBr_4 is based on how close theoretical approximations for χ are to experimental measurements. Experimentalists measure the susceptibility of this material by placing it in a constant magnetic field and then measuring the magnetization as the temperature is varied. This experiment was carried out for Cs_2CuBr_4 in a constant magnetic field of 1 Tesla applied along three different axes of the crystal; the susceptibility was measured along these three different axes [1]. The results are illustrated in figure 13. We obtained the experimental data for χ from the authors of [1], and I use them in my analysis.

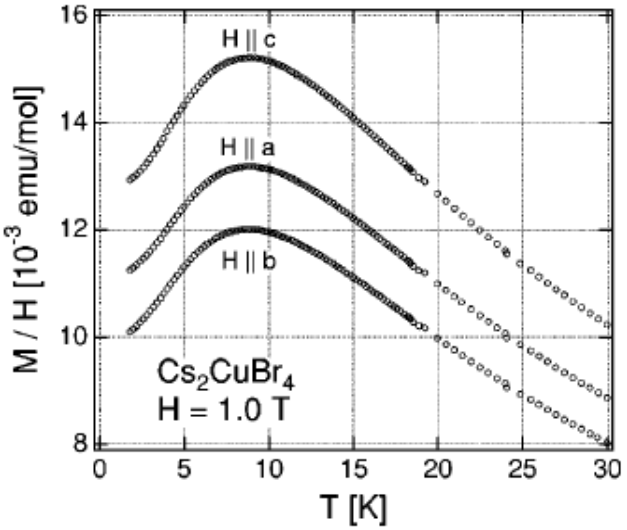

FIG. 13. [1] The susceptibility of Cs_2CuBr_4 as a function of temperature in a magnetic field of 1.0 T, applied parallel to each of its axis.

We next want to find a suitable theoretical approximation of the susceptibility. The |3,5| and |4,4| D-Log Padé approximants of χ are the only approximants that exhibit the characteristic behavior of the experimental susceptibility curve (see figure 13). Thus, either of them is suitable to use for further analysis. I chose to use the |4,4| D-Log Padé approximant. Using the |3,5| D-Log Padé approximant instead of the |4,4| one, will not change the results much since the S^2 value[{6}], between these curves, with $J_1/J_2=0.5$ (see footnote 4) is on the order of 10^{-5} indicating the curves are for the most part identical.

Plotting out the |4,4| D-Log approximant of χ against the H||c experimental susceptibility data produces a theoretical susceptibility curve which does not agree well with the experimental one. However, if the theoretical curve is translated along the T axis by J units, and by B units in the χ direction, the theoretical fit can be improved. Figure 14 illustrates one such translation.

[{6}] See section 10 for a discussion on least squares (S^2) analysis.

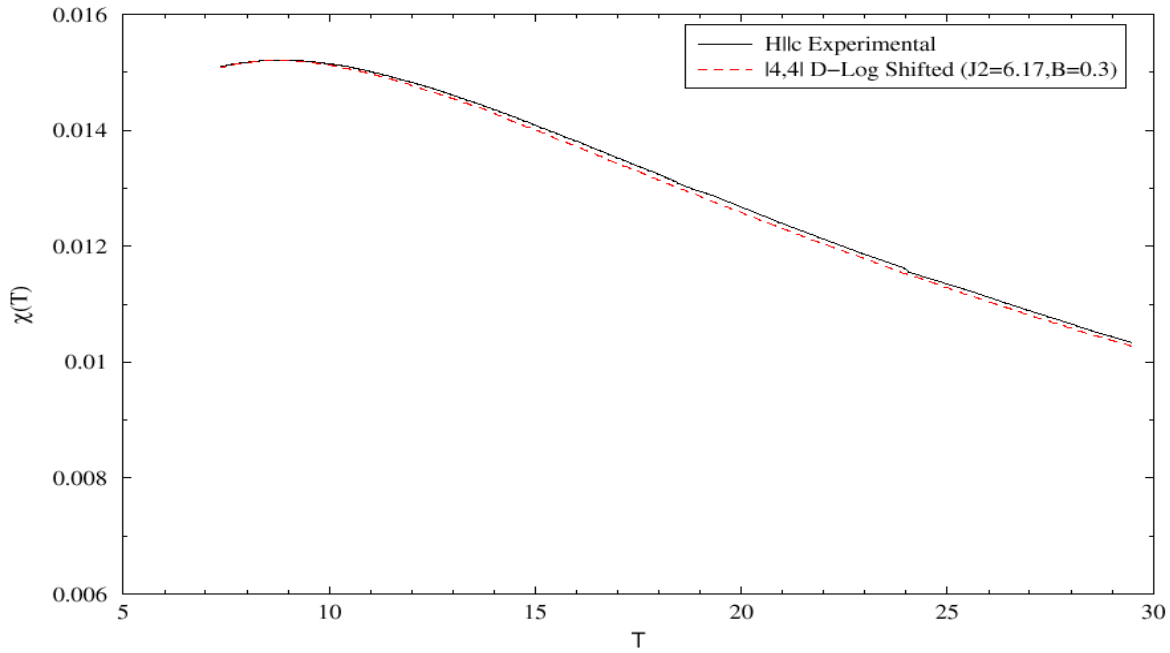

FIG. 14. The theoretical curve can be translated along each axis to improve the fit. This is illustrated here where J(= J_2) = 6.17, B = 0.3, with J_1/J_2 = 2.3. Again, the choice of J_1/J_2 = 2.3 is arbitrary.

It turns out that the number of temperature units (J) the theoretical curve is shifted by is the nearest neighbor exchange constant J_2 (see figure 4). Furthermore, the number of units shifted in the χ direction (B) is directly related to the Lande factor by,

$$g = \sqrt{\frac{B\, k_B\, J_2}{N_A\, \mu_B}} \tag{35}$$

Let the inverted (see section 8) D-Log Padé approximant for χ be called χ_{model}. This is not the molar susceptibility since it does not have the correct units. We need to multiply χ_{model} by some constants to obtain χ_{molar}, which is the physical quantity of importance. When χ_{model} is shifted by J_2 along the temperature axis, Program 1 defines the relationship between the shifted χ data (call it χ_{shift}) and the molar susceptibility as,

$$\chi_{molar} = \frac{N_A g^2 \mu_B{}^2}{k_B J_2} \chi_{shift}(T \times J2) \tag{36}$$

Furthermore, we have the relation χ_{molar} = B χ_{shift}; Plugging (36) in for χ_{molar} and solving for g gives us (35). In effect, shifting the theoretical curve determines the exchange constant J_2 and g (via (35)) directly. J_1 is found by multiplying J_2 by the ratio J_1/J_2, which is known from the outset.

The problem at hand is to choose J_2 and B sufficiently so that the theoretical approximation of χ produces the closest fit possible to the experimental data for any given value of J_1/J_2. The parameters which produce the best fit plot are then taken to be the exchange constants and g factors present in Cs_2CuBr_4.

10. Computer Program Used to Determine the Best Fit Theoretical Curve, and the Results it Implies

The process of determining J_1, J_2, H_s, and g factors that yield the best fit theoretical χ curve to the experimental χ curve is too tedious to do manually. The most efficient way to perform this data analysis is to write a computer program which varies J_2 and B little by little over a sufficient range of values, to determine which set of parameters produce the best fit curve using a |4,4| D-Log Padé approximant of χ. This was my major task. I wrote a C language computer program to perform this data analysis[7]. I will only discuss its main features. The entire source code is given in Appendix B.

First, the experimental and theoretical data sets are scanned into 4 separate arrays, one for each quantity. As mentioned before, the theoretical values are from the |4,4| D-Log Padé approximant for a given J_1/J_2 value and are in the form β vs. $T^*\chi(\beta)$. In the next operation, the data is inverted to produce theoretical data sets of the form T vs. $\chi(T)$. Figure 14 illustrates a susceptibility curve after it has been inverted. An algorithm next determines the maximum χ value, and the temperatures at which they occur, for the experimental and theoretical curves. Call these values $\max(\chi_{exp})$, $\max(T_{exp})$, $\max(\chi_{theo})$, and $\max(T_{theo})$[8]. The theoretical curve is then shifted by B_{max} in the χ direction and by J_{2max} in the T direction, where $J_{2max} = \max(T_{exp})/\max(T_{theo})$ and $B_{max} = \max(\chi_{exp})/\max(\chi_{theo})$. This translation shifts the theoretical curve such that its peak matches the peak of the experimental curve.

Once the data is shifted, the remainder of the operations in the program is carried out for a range of J_2 and B values. These ranges are defined as $[J_{2L} \le J_{2max} \le J_{2U}]$ and $[B_L \le B_{max} \le B_U]$, where the subscripts L and U represent the lower and upper boundaries respectively. I used a symmetric interval for the range of J_2 and B values, where $J_{2L} = J_{2max} - 5.0$, $J_{2U} = J_{2max} + 5.0$, $B_L = B_{max} - 1.0$, and $B_U = B_{max} + 1.0$. I chose these ranges by examining the best fit curves for values both inside and outside these intervals. I noticed that for values outside of these intervals, the fits progressively worsened, while values within these ranges produced better fits. Using a "for" loop, J_2 is varied from J_{2L} to J_{2U}, incremented by a given value ΔJ_2, each time through the loop. Within this loop, a second "for" loop varies B from B_L to B_U, incremented by some ΔB, each time through this loop. I determined ΔJ_2 and ΔB by examining how big a change in J_2 and B needed to be made to produce a significant change in the fit. I found $\Delta J_2 = 0.01$ and $\Delta B = 0.001$ to be sufficient step sizes.

For each value of J_2 and B within the abovementioned ranges, each of the following operations are carried out. First, the g factor is calculated using (35). J_1 and J_2 are then converted from units of Kelvin to units of meV[9]. The saturation field H_s is next computed using the relation,

---

[7] I would like to thank Dr. Nick Puketza of the UCD Department of Computer Science for very helpful discussions regarding my program.

[8] exp = experimental and theo = theoretical

[9] 1 meV = 11.604 K

$$H_s = \left[2J_1 + 2J_2 + \frac{J_2^{\,2}}{2J_1} \right] \times \frac{\gamma}{g} \qquad (37)$$

where γ is a conversion to units of Teslas[{10}]. The saturation field was determined experimentally to be ~30 Teslas for H||a and H||b, and ~28 Teslas for H||c [1]. Using these values as a guide, a tolerance is placed on H_s. Thus allowable J_1, J_2, and g values are limited to those which satisfiy: ($30.0 \leq H_s \leq 32.0$) for H||a and H||b, and ($28.0 \leq H_s \leq 30.0$) for H||c. For those J_2 and B values which satisfy the constraints on H_s, their corresponding shifted data is then inverted to have χ(T) at discrete temperature values.

At low temperatures, the reliability of the D-Log Padé approximants begins to break down at ~0.3 temperature units below the peak value (see section 8). However, if the theoretical data is shifted by for example J=6.0, the "range of reliability" of the approximant becomes 0.3 x 6.0 = 2.0 temperature units below the peak. For each ratio of exchange constants examined, J_{max} is approximately 6.0. From figure 13, we see that the peak occurs at T ~ 9; thus, the shifted theoretical data is taken to be reliable down to T = 7. In my program, each data set is limited to a temperature range between 7 and 30. The upper limit of 30 for the range is somewhat arbitrary, since we know that for high T the approximations are accurate. Figure 14 shows that the upper limit of 30 is sufficient since the theoretical and experimental curves both behave in the same linear, Curie-like fashion beginning at about T = 15 and continuing up to 30.

A problem arises. The D-Log Padé approximants result in values of χ at 10,000 temperature steps, while the experimental measurements of χ were only taken for 239 temperature values. The temperature limitations described above decreases the number of experimental data points to about 80, but there are still thousands of theoretical data points which lie in the allowed temperature region. To construct like data sets, an algorithm first truncates the data sets by imposing the temperature limitations. Next, each theoretical T value is compared to each experimental T value; only the matching temperature values and their respective χ values are then recorded into separate arrays, ultimately weeding out all unmatched theoretical data points.

Using a temperature step of 0.00001 in the Padé approximant produces a second problem. With such a small temperature step, and experimental temperatures reported to only 2, 3, or 4 decimal places, some temperature values in the theoretical data set are repeated, giving different values of χ for the same T value. Figure 15 is an excerpt from a theoretical data set illustrating this issue.

[{10}] γ = 17.276 Tesla

T	χ(T)	T	χ(T)	T	χ(T)
…	…	…	…	…	…
22.96	0.011382	12.98	0.013250	7.99	0.013302
22.96	0.011383	12.98	0.013251	7.99	0.013303
22.47	0.011483	12.98	0.013250	7.99	0.013302
21.95	0.011588	12.98	0.013251	7.99	0.013301
21.95	0.011590	12.98	0.013252	7.99	0.013302
21.38	0.011706	12.79	0.013272	7.99	0.013301
21.38	0.011708	12.79	0.013273	7.99	0.013303
20.95	0.011795	12.79	0.013274	7.99	0.013302
20.95	0.011796	12.79	0.013273	7.99	0.013301
…	…	…	…	…	…

FIG. 15. Excerpt of an intermediate output file illustrating the occurrence of multiple T values with different χ values. The χ values are averaged out for like T values, and are then taken to be the susceptibility at that temperature.

This problem results from round off errors created by discrepancies in the precisions of theoretical and experimental T values. To fix this problem, an algorithm scans through the theoretical data arrays and finds the T values that match, averages out their respective χ values, and records them into a separate array.

The data manipulation thus far has created two data sets; one which gives experimental values of χ, and another giving approximates of χ, for a set of T values between 7 and 30. These sets are created for given J_2 and B values each time through the loop. Now that we have these two sets of data, we can determine how close the theoretical data fits the experimental data. The notion of closeness here is measured in the S^2 sense. The S^2 value for a given set of experimental and theoretical data, is a function of J_2 and B and is defined by,

$$S^2(B, J_2) = \sum_i (e_i - t_i)^2 \tag{38}$$

where e_i and t_i are the experimental and theoretical χ values at the i^{th} temperature step. The sum over i extends over the number points in the sets. The S^2 value is a measure how big the difference is between the curves; the smaller the S^2 value the better the fit.

The program next calculates the S^2 value for each J_2 and B. The program then keeps track of which J_2 and B value produces the smallest S^2 value. In this algorithm, the quantity S^2/m (m = number of data points) is also calculated; this is the average S^2 value per point. The minimum of this quantity is also found using the same algorithm that tracks the minimum S^2 value. The S^2/m value is calculated to into account that there are varying number of data points for different values of J_2 and B.

After termination of the program, three important text files are created. First, S2vals.txt, lists the S^2 and S^2/m values for each J_2 and B value tested. An excerpt from one of these files is shown in figure 16.

J_2	B	S^2	S^2/m	m
5.30	0.26326	4.258547E-05	5.193350E-07	82
5.30	0.26426	3.819798E-05	4.658290E-07	82
5.30	0.26526	3.415988E-05	4.165839E-07	82
5.30	0.26626	3.046077E-05	3.714728E-07	82
5.30	0.26726	2.709536E-05	3.304312E-07	82
5.30	0.26826	2.406405E-05	2.934640E-07	82
5.30	0.26926	2.136929E-05	2.606011E-07	82
5.30	0.27026	1.901030E-05	2.318329E-07	82
…	…	…	…	…

FIG. 16. Sample output of S2vals.txt file, listing the S^2 and S^2/m values for each J_2 and B value tested.

Second, FINALexp.txt and FINALtheo.txt list the data sets for each value of J_1 and B. Figure 17 illustrates a section of the FINALtheo.txt file.

J1=	12.72	J1=	12.72	J1=	12.72
B=	0.228	B=	0.238	B=	0.248
T	CHI(T)	T	CHI(T)	T	CHI(T)
29.46	0.007025	29.46	0.00733	29.46	0.00764
28.95	0.007105	28.95	0.00742	28.95	0.00773
28.46	0.007180	28.46	0.00749	28.46	0.00781
27.97	0.007259	27.97	0.00758	27.97	0.0079
27.46	0.007342	27.46	0.00766	27.46	0.00799
26.45	0.007512	26.45	0.00784	26.45	0.00817
25.97	0.007594	25.97	0.00793	25.97	0.00826
25.46	0.007684	25.46	0.00802	25.46	0.00836
24.85	0.007793	24.85	0.00813	24.85	0.00848
…	…	…	…	…	…

FIG. 17. Sample output of FINALtheo.txt file. The theoretical data sets are listed for every step in J_1 and B.

Finally, gvalues.txt lists the J_1, J_2, g, H_s, S^2, S^2/m, and m values for the best fit theoretical curve, for each value of J_1/J_2. We then take the parameters J_1, J_2, g, and H_s, which result in the smallest S^2 or S^2/m values, to be the quantities that exist in Cs_2CuBr_4. Once we know the overall best fit parameters, their respective data sets are found in FINALexp.txt and FINALtheo.txt. A plotting routine is then used to produce plots of the experimental and best fit theoretical $\chi(T)$ curves.

11. Discussion and Results

Previous studies of Cs_2CuBr_4 used a different approach to determine the exchange constants in this material [1]. In this study, Neutron elastic scattering experiments determine

the ordering wave vector, $\mathbf{Q}_0 = (0,Q_0,0)$. Classically, the ordering wave vector is related to the exchange constants by,

$$\cos(Q_0\pi) = -\frac{J_2}{(2J_1)} \tag{39}$$

In the ordered phase of Cs_2CuBr_4, $\mathbf{Q}_0 = (0,0.575,0)$ and $J_1/J_2 = 2.1$ [1]. Using these quantities along with $gH_s \approx 63T$ and the relation,

$$g\mu_B H_s = 2J_2[1-\cos(Q_0\pi)] + J_1[1-\cos(2Q_0\pi)] \tag{40}$$

they found that $J_1 = 13.9$ K and $J_2 = 6.5$ K, for Cs_2CuBr_4 [1] {11} .

We are now equipped to compute J_1, J_2, the g factors, and H_s for Cs_2CuBr_4 using our model. First, program 1 is used to generate the coefficients in the expansion (25) for the ratios J1/J2 =0.0, 0.1, 0.2…5.0. Second, program 2 is used to generate a |4,4| D-Log Padé approximant for the susceptibility using each value of the ratio of the exchange constants, for 10,000 steps in β. Finally, I ran my program for each ratio of exchange constants, tested against the three different sets of experimental data for Cs_2CuBr_4 (One set for each direction, i.e. H||x). The results are given in Appendix C, which report the parameters yielding the best fit theoretical curve for each J_1/J_2 {12} .

We established that Padé approximants are not as reliable as the D-Log Padé approximants. Thus, the values in Appendix C are not taken as the quantities that best describe the properties of Cs_2CuBr_4. However, the tables in Appendix C gives us a good idea as to which values of J_1/J_2 will produce the best fits; allowing us to narrow down the range of possible best fit values of J_1/J_2, when we use D-Log Padé approximants instead. The same procedure from above is implemented for various values of J_1/J_2 using D-Log Padé approximants; the results are reported in Appendix D{12}.

As a simple check of the best fit parameters, the best fit J_1 and J_2 values should remain the same despite the direction of the applied magnetic field, and the g factors should differ in each direction since it is an anisotropic quantity. The overall best fit curve for each direction is produced when $J_1/J_2 = 2.3$. The best fit curves for: H||a has $J_1 = 14.4$, $J_2 = 6.3$, $g_a = 2.094$ and $H_s = 30.4$, H||b has $J_1 = 14.4$, $J_2 = 6.3$, $g_b = 1.998$ and $H_s = 31.9$, H||c has $J_1 = 14.4$, $J_2 = 6.3$, $g_c = 2.248$ and $H_s = 28.4$. Each of these fits has $S^2/m \sim 10^{-10}$. Thus the results pass our "simple check" as expected. Figure 18 is a plot of the best fit susceptibility curves for each direction of the applied field.

{11} I have assumed a factor of 2 difference in their definition of the exchange constants.
{12} The overall best fit parameters are highlighted in red.

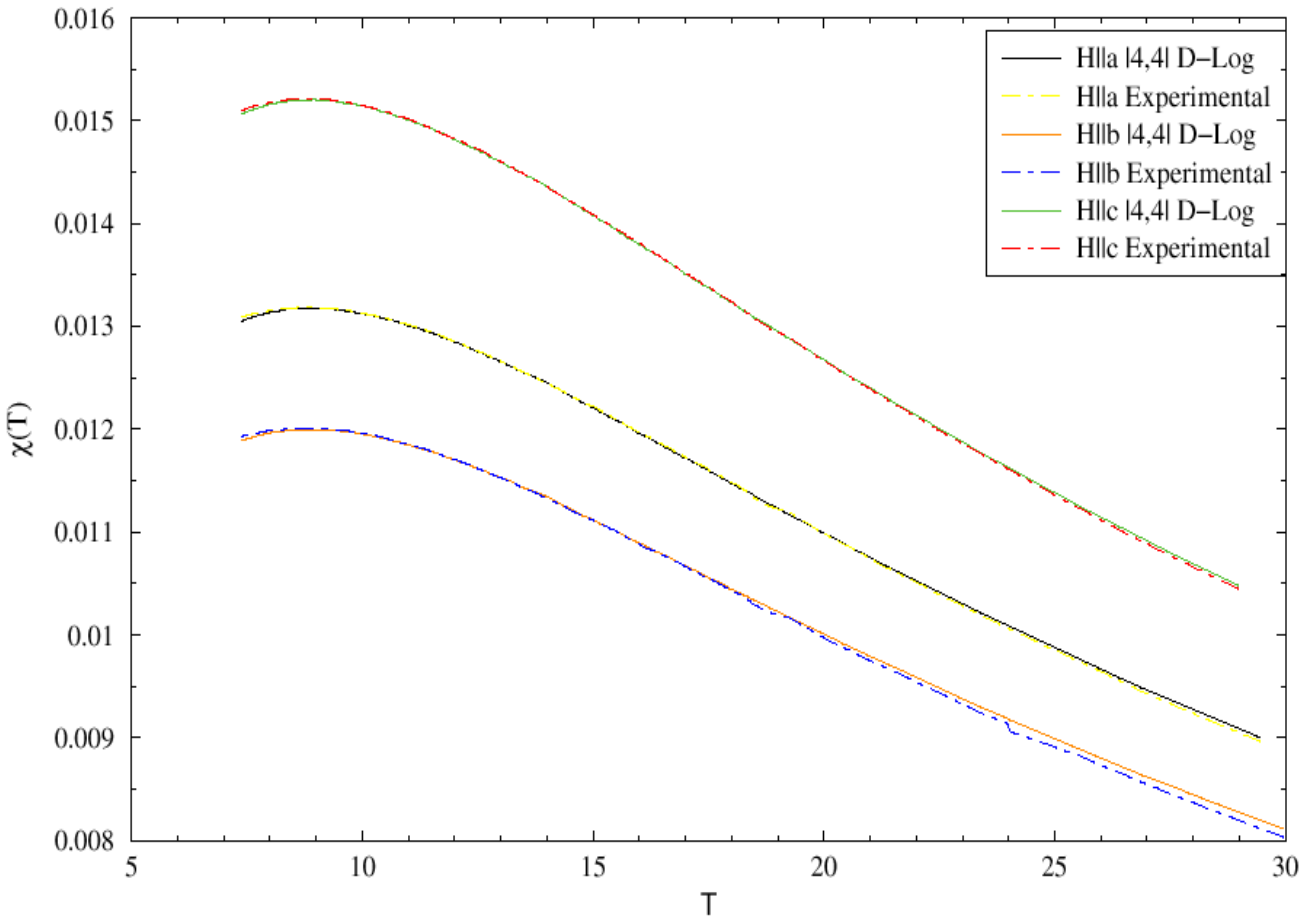

FIG. 18. Best fit theoretical χ curves with an applied field in the a, b, and c directions of the Cs_2CuBr_4 crystal (See figure 12). (Note the axes do not cross at zero). The actual deviations of these curves are measured in the S^2 sense and are reported in Appendix D.

The authors of [1] report that the saturation field for the a and b directions should actually be between 30 and 31 Teslas while the saturation field for the c direction should be between 28 and 29. The values we find satisfy these criteria in the a and c directions but not for the b direction. It turns out that the without allowing the saturation field, for the b direction, to be higher than 31 we cannot obtain a good fit; this is illustrated in figure 19 where we constrained $J_1 = 13.9$ and $J_2 = 6.5$, as reported in [1], constrained H_s to be in the range 30 - 31 for the a and b directions, and 28 - 29 for the c direction; the g values for each direction are allowed to vary freely.

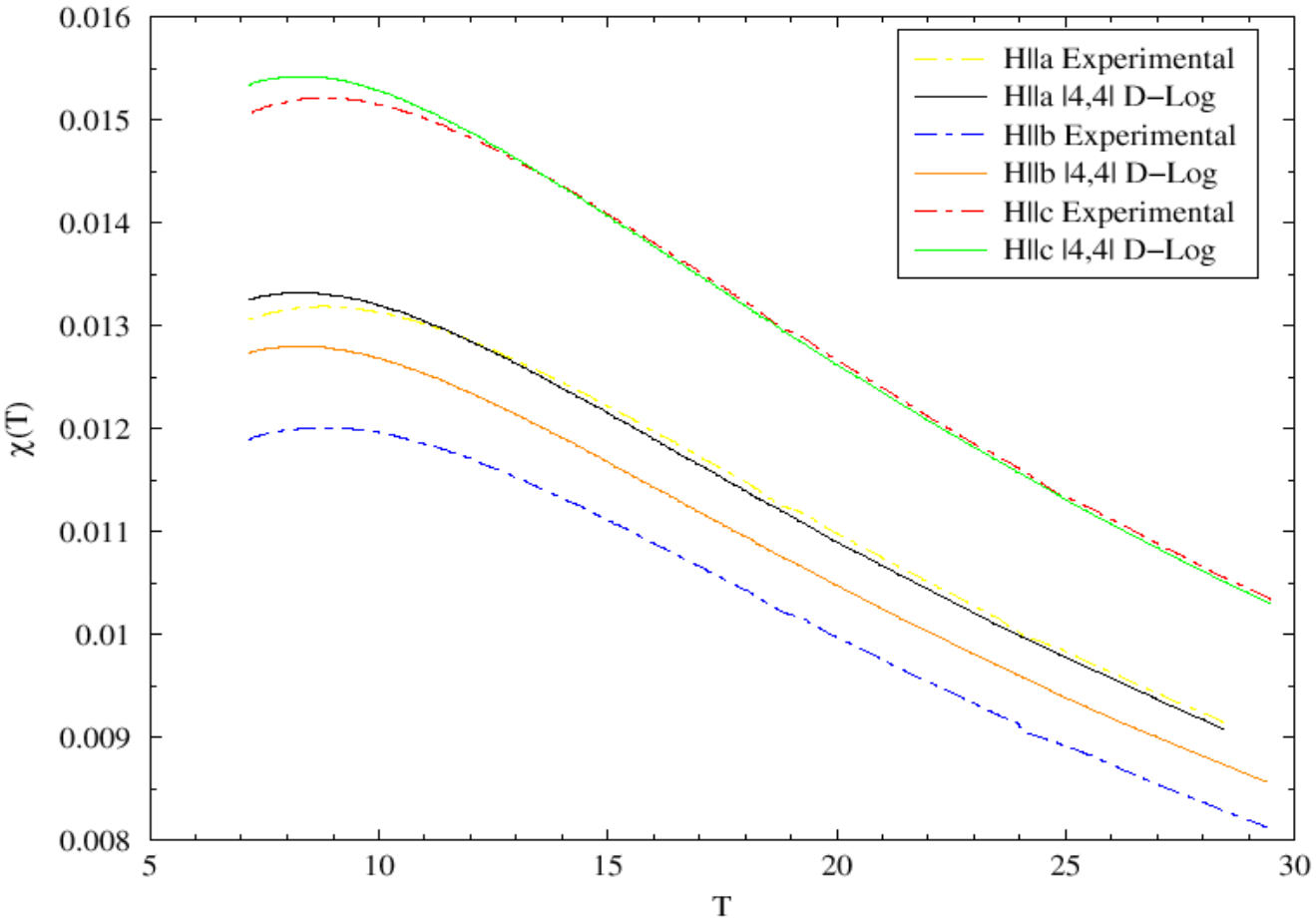

FIG. 19. Best fit plot when reported constraints [1] are placed on J_1, J_2, and the H_s's. The H||b |4,4| D-Log approximant curve cannot be improved beyond this without allowing the saturation field for the b direction to be larger than 31. The H||a and H||c D-Log approximants have $S^2 \sim 10^{-9}$ while the H||b D-Log plots have $S^2 \sim 10^{-7}$.

These plots are obviously nowhere near as good of fits as those shown in figure 18; they can however be improved, but only if the saturation field in the b direction is allowed to be larger than 31.

Our theoretical calculations of J_1 and J_2 differ from the experimental determinations of these quantities by 0.5 K and 0.2 K respectively. The ratio of the exchange constants predicted by our theoretical model is also higher by about 0.2. A possible reason for the discrepancies in our theoretical results could be because we treated the magnetic unit cells as two dimensional ones; that is, we disregarded (inter-planar) exchange interactions between the ions in adjacent planes. Neutron scattering experiments found that inter-planar exchange interactions are on the order of $10^{-2} \times J_1$ in Cs_2CuBr_4 [1]; this implies they are relatively small compared to exchange interactions occurring within the planes. However, this material is indeed 3 dimensional and including these interactions might bring our results closer to those reported in [1]. It is a difficult task to take these types of interactions into account. In this case, the Hamiltonian in (5) has a third exchange interaction term in it making it even more difficult than before (when there were only two terms in the Hamiltonian) to compute the coefficients in (25); the complication arises from the exponentiation of a non-diagonal Hamiltonian.

12. Conclusions

In this paper, I discussed recent advances regarding the properties of spin-½ TAF's including the effect of frustration on magnetic ordering, and applications of high temperature series expansions of the magnetic susceptibility. Furthermore, I wrote a C language program, that uses least squares analysis, to determine the exchange constants, Lande factors, and the saturation field for the real spin-½ Cs_2CuBr_4. This program computes these quantities based on analysis of D-Log Padé approximants of high temperature series expansions of the magnetic susceptibility, for the Heisenberg model of an anisotropic spin-½ TAF.

Our theoretical analysis using the Heisenberg model for an anisotropic spin-½ TAF finds that J_1=14.4 and J_2=6.3 in Cs_2CuBr_4. Our results are in relatively good agreement with experimental results; in obtaining these values however, we allowed the saturation field to be larger, for the b direction, than what is reported for Cs_2CuBr_4 in [1]. Restricting all the parameters to those reported in [1] did not produce good fits. Treating the system as a three dimensional spin-½ antiferromagnet instead of a spin-½ triangular antiferromagnet could possibly resolve the discrepancies in our results; this is a valid avenue for further research in this field.

Acknowledgements

I would foremost like to thank Dr. Rajiv Singh for giving me this wonderful opportunity to work with him to study recent developments in magnetism. I am grateful for the countless hours of help and guidance he so willingly and enthusiastically dedicated to helping me with this project. It was truly a great experience. Thank you so much for all of your help and support!!!

References

Papers:

[1] T. Ono et al, Phys. Rev. B **67** 104431 (2003)

[2] U. Schotte et al, J. Phys. Condens. Matter **6** 10105-10119 (1994)

[3] Z. Weihong, R. H. McKenzie, R. R. P. Singh, Phys. Rev. B **59** 14 367 (1999)

[4] N. Elstner, R. R. P. Singh, A. P. Singh, Phys. Rev. Lett. **71** 1629 (1993)

[5] M. Tamura, R. Kato, J. Phys: Condens. Matter **14** L729-L734 (2002)

[6] S. Eggert, I. Affleck, M. Takahashi, Phys. Rev. Lett. **73** 332 (1994)

[7] J.K. Kim, M. Troyer, Phys. Rev. Lett. **80** 2705 (1998)

Texts:

1. M. Toda, R. Kubo, N. Saitô: Statistical Physics I: Equilibrium Statistical Physics (Springer-Verlag 1983)

2. R. Bowley, M. Sanchez: Introductory Statistical Mechanics 2nd Edition (Clarendon Press, Oxford 1999)

3. N. W. Ashcroft, N. D. Mermin: Solid State Physics (Holt, Reinhart, and Winston 1976)

4. H. C. Ohanian: Principles of Quantum Mechanics (Prentice Hall 1990)

5. D. D. Ebbing, S. D. Gammon: General Chemistry 6th Edition (Houghton Mifflin Company 1999)

6. D. C. Mattis: The Theory of Magnetism I: Statics and Dynamics (Springer-Verlag 1981)

7. M. A. Omar: Elementary Solid State Physics: Principles and Applications (Addison-Wesley Publishing Company, Inc. Reprint 1993)

8. C. Kittel: Introduction to Solid State Physics 3rd Edition (John Wiley & Sons, Inc. 1966)

9. R. L. Burden, J. D. Faires: Numerical Analysis 7th edition (Brooks/Cole 2001)

10. S. Chikazumi, S. H. Charap: Physics of Magnetism (John Wiley &Sons, Inc. 1964)
11. H. E. Hall: Solid State Physics (John Wiley & Sons, Inc. 1974)

12. R. Celotta, J. Levine: Methods of Experimental Physics Part A: Neutron Scattering (Academic Press, Inc. 1986)

13. D. J. Griffiths: Introduction to Electrodynamics (Prentice Hall, reprint 1999)

14. G. A. Baker, JR.: Essentials of Padé Approximations (Academic Press, 1975)